EUROPEAN ORGANIZATION FOR NUCLEAR RESEARCH
ORGANISATION EUROPEENNE POUR LA RECHERCHE NUCLEAIRE

CERN - PS DIVISION

PS/ AR/ Note 95-12

BEAM LIFETIME TESTS FOR Pb^{52+}, Pb^{53+} and Pb^{54+} IONS SUBJECT TO ELECTRON COOLING IN LEAR (PERFORMED IN JUNE 1995)

S. Baird, J. Bosser, C. Carli, M. Chanel, P. Lefèvre, R. Ley, R. Maccaferri,
S. Maury, I. Meshkov, D. Möhl, G. Molinari, F. Motsch, H. Mulder,
G. Tranquille, F. Varenne

Geneva, Switzerland
26 September 1995

LIST OF CONTENTS

1. INTRODUCTION

LEAR is expected to be used as a lead ion accumulator in the framework of the LHC project [1]. For that purpose the electron cooler plays an important role in the stacking process [2].

First tests, made in December 1994 [3] with Pb^{53+}, have shown that the ion lifetime is in the order of 2 to 4 seconds with an electron-cooler current of 0.4 A and under "normal" physical ($P \approx 2 \times 10^{-11}$ torr) vacuum conditions. This relatively short lifetime is supposed to be due to the recombination (radiative and/or dielectronic) of the ions with the electrons of the cooling beam[4]. The transverse cooling time is expected to be in the order of 0.2 s while the stacking process should take about 2 s. Hence the short lifetime of the Pb^{53+} beam was considered as a serious difficulty.

A rough analysis of the atomic levels and the ionization potentials of lead [Appendix 1] convinced us that Pb^{54+} and Pb^{52+} might be less vulnerable to recombination with the comoving electrons. It was therefore decided to concentrate the June 1995 experiment, which is the subject of the present paper, to comparative lifetime measurement of cooled Pb^{52+}, Pb^{53+}, and Pb^{54+}.

This note will first give a brief description of the experimental set-up i.e. of the main parameters of the ion injector, LEAR and the LEAR diagnostics. Then the lifetime measurements and a rough estimate of the transverse cooling time will be given. Finally proposals will be made for future experiments.

2. CHARACTERISTICS OF THE LEAD ION BEAM FROM THE LINAC

The lead ions (Pb^{27+}) accelerated to 4.2 MeV/u in Linac 3 [5] are stripped by a foil at the exit of the linac. The intensities of the different charge states obtained after the stripper vary with the thickness of the stripping foil, but with the "optimum" thickness about equal intensities of Pb^{52+}, Pb^{53+} and Pb^{54+} were obtained (Fig. 1) in fair agreement with the results of [6]. A single charge state is selected in a filter line by adjusting the bending magnets of a "dogleg" arrangement and a narrow momentum defining slit. The available current after the filter line is about 20 to 25 μA. The pulse length has been reduced from 400 μs to 20 μs (as mainly single-turn injection with a length of ≈2 μs was used but the possibility to inject more turns was retained). Parameters of the linac beam are given in Table 1.

Table 1. Linac beam parameters.

Energy	4.2 MeV/μ
Velocity factor β	0.094
Beam current (after stripping to 52+, 53+, or 54+)	20 - 25 μA
Corresponding number of ions	2.3 - 2.8 × 10^6 ions/μs

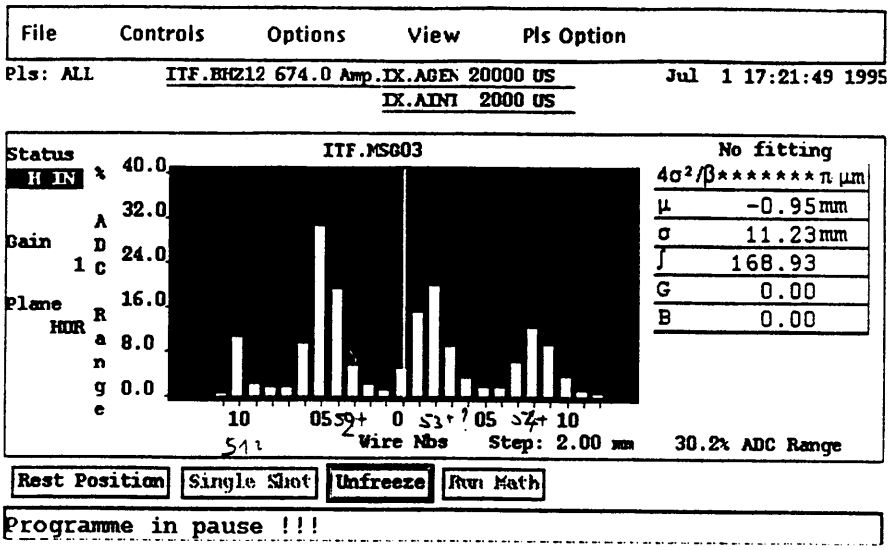

Fig. 1 - Different charge states seen in a SEMgrid of the filter line

3. INJECTION OF LEAD IONS INTO LEAR

3.1 Matching of the E0 Line

The efforts made to adjust the Twiss parameters at the entrance of the E0 line had no success. Reasons are :

- The method of variation of the quadrupole whilst currents recording of the rms width of the beam on a semgrid is efficient if the beam has a width greater than the resolution of the grid (at least 3 bins per sigma). This will be solved for the next MD by using semgrid 11 which has a very fine wire spacing and can be rotated so that measurements in both transverse planes can be made.
- Semgrid 15, which was mainly used in the present measurements was not at the expected place. In fact its electronic was connected to semgrid 12. This was only discovered after the experiment. Semgrid 12 is 1 m downstream the last triplet before the E0 line while semgrid 15 is 5 m downstream. Therefore, our calculations were based on a wrong assumption.

3.2 E0 and E2 Lines

For the 3 charge states we have succeeded to have particles at the exit of the line despite the saturation of some of the magnets. The matching at the exit of the line was not correct due to the difficulties discussed above.

No major problem was encountered to steer and to focus the beam in the E2 line.

3.3 Injection into LEAR

There were difficulties to have a good matching at injection into LEAR. But we always succeeded to inject between 2×10^7 and 10^8 charges/injection. The injection used was one-turn

injection. Normally we should inject about 2×10^8 charges. Multi-pulse injection was tried and a maximum of 10^9 charges of Pb^{52+} were injected by bunching the cooled stack over a fraction of the circumference and injecting the new pulse onto the free part. As the lifetime measurements could be performed with the relatively low intensity, efforts to improve the intensity by better matching and stacking were not pursued further.

4. LEAR VACUUM

The LEAR vacuum was measured at several locations by using 18 Bayard-Alpert gauges installed around the ring. The gas composition was also recorded at 4 different places in the machine where residual gas analyzers are installed.

The average partial physical pressure for hydrogen was about 1.2×10^{-11} torr, and the other gases participate for about 0.6×10^{-11} torr (Table 2). The calculated lifetime (Table 2) using the estimated vacuum conditions and Franzke's formula [7] is around 18 s, in agreement with our lifetime measurements. The exact agreement is accidental since the gas composition is only known in 4 points and large variations can occur between these locations.

Table 2 - Estimate of LEAR vacuum conditions and calculated lifetime from Franzke's formula

		SECTOR:	102		204 ***		303		304			Ring averages		
		Length[m]	50		50		4		4					
Rest gas	Lifetime for 10^{-11} torr		P*	<P>**	P	<P>	P	<P>	P	<P>	<P> ring	Rel. <P> ring	$1/t_{life}$	t_{life}
H_2	625		16.	10.19	5.1	3.25	16.	0.81	6.1	0.31	14.56	0.73	0.023	42.9
He	624		0.6	0.38	1.3	0.83	3.1	0.16	9.4	0.48	1.85	0.09	0.003	338.0
CH_4	126		0.4	0.25	1.6	1.02	1.1	0.06	1.1	0.06	1.39	0.07	0.011	91.2
H_20	129		0.72	0.46	1.4	0.89	0	0.00	1,1	0.06	1.41	0.07	0.011	91.5
N_2	92		0	0.00	0	0.00	0	0.00	2.	0.10	0.10	0.01	0.001	903.2
CO	92		0.2	0.13	0.28	0.18	0.85	0.04	0	0.00	0.35	0.02	0.004	263.2
Ar	76		0	0.00	0.21	0.13	0	0.00	0.17	0.01	0.14	0.01	0.002	533.9
CO2	59		0	0.00	0.16	0.10	0	0.00	0.13	0.01	0.11	0.01	0.002	540.3
Sum											19.90		0.057	
*P = Partial physical pressure in 10^{-11} torr											Final t_{life} (sec) = 17.6			
**<P> = contribution of this section to the average pressure of the ring														
***Note: 50 m is 10 m for sector 2 and 40 m for section 4 where vacuum is 4 times worse														

5. LEAR BEAM DIAGNOSTICS

5.1 Ion Beam Diagnostics

5.1.1 Lifetime diagnostics

Due to the low number of stored particles the classical intensity and closed orbit measurements were not available.

The relative ion beam intensity versus time was estimated using the output signal of a longitudinal Schottky pick-up processed by a spectrum analyzer (HP 8568A). Since the ion beam density is rather small (no appearance of the usual double-peaked signal with electron cooling) the power of the Schottky signal is directly proportional to the number of stored ions. Therefore, its evolution in time gives a good estimate of the lifetime. The Schottky noise is acquired from the spectrum analyzer output port and processed by a laptop computer.

The spectrum analyzer is used in receiver mode (i.e. in time domain). The frequency at which the analyzer was set ($f \approx 36$ MHz) was chosen at the 100th harmonic of the revolution frequency and a resolution bandwidth of 30 kHz was used in order to record the integrated signal density in a frequency range covering the beam momentum spread $\cong 10^{-3}$. Then the integrated Schottky noise power $S^2(t)$ in the band can be deduced, which is a good measure of the beam current. The electronic noise (N) of the acquisition system adds in square to the Schottky signal. Hence the voltage recorded by the analyzer is $U(t) = \sqrt{S^2(t)+N^2}$ and the lifetime τ can be obtained from $U(0) = \sqrt{S^2(0)+N^2}$ and $U(\tau) = \sqrt{S^2(0)/e + N^2}$ by determining the time span between the readings $U(0)$ and $U(\tau)$, where the beginning (t=0) was chosen about 1 sec after injection so that the beam was already well cooled at the start of the lifetime measurement.

An example of measurement after processing by the laptop computer is given in Fig. 2.

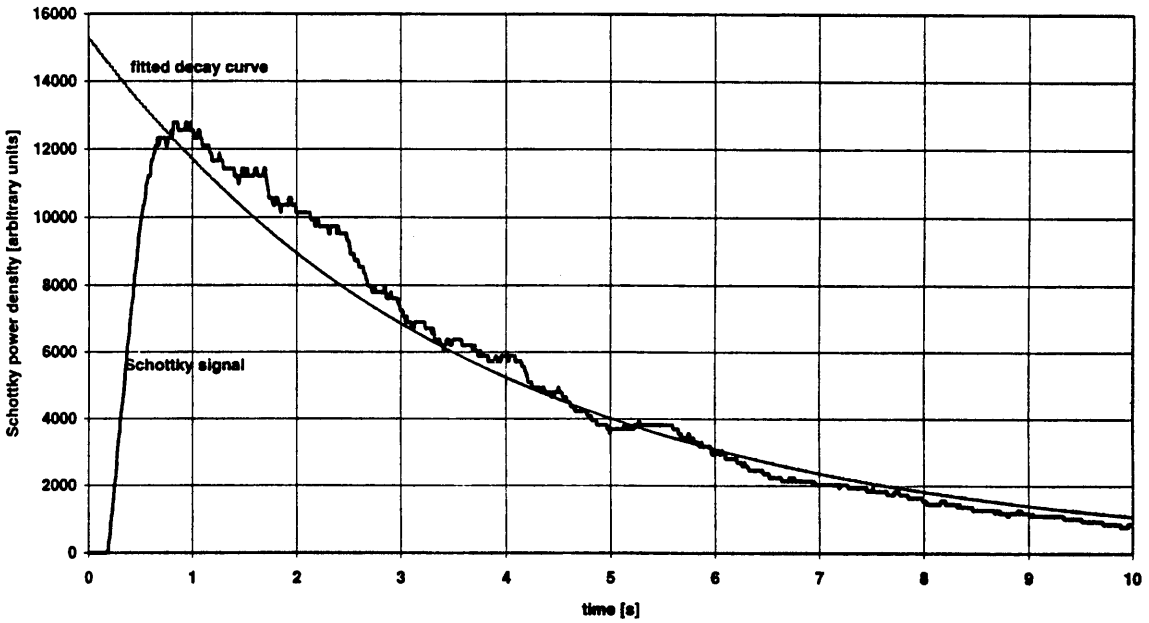

Fig. 2 - Variation of the Schottky power density at 36.097 MHz as a function of time

5.1.2 Transverse cooling time diagnostics

The horizontal and vertical dimensions are measured by beam ionization profile monitors (BIPM/H and BIPM/V) triggered at injection. These devices are processed by a front-end microprocessor. The resolution of the collecting grids is 1 mm. Despite the small intensity and

the low residual pressure the measured data were sufficient for a rough estimate of the transverse cooling time and accurate enough to give evidence of good beam cooling at the time of the lifetime measurement. The signals from the collecting grids are integrated during fixed-time intervals which were chosen to be 100 ms for the purpose of our experiments. The integrated spatial distributions were acquired via an RS232 port to a PC to provide an estimate of the rms beam width as a function of time.

An example of the horizontal dimension versus time, for Pb^{54+}, is given in Fig. 3. The time difference between each profile is 100 ms and the electron beam intensity is I_b = 120 mA.

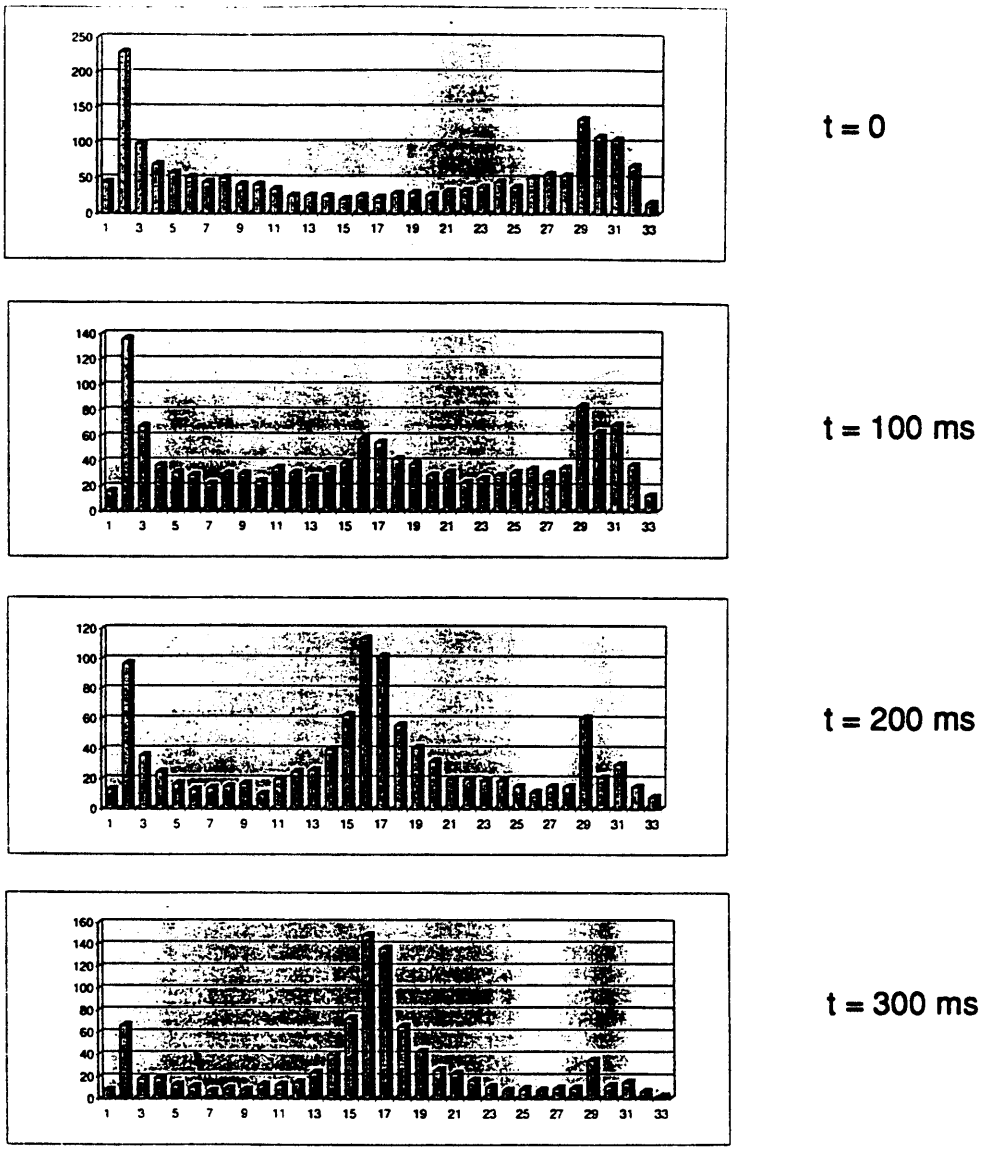

Fig. 3 - Evolution of the horizontal beam profile during the first 300 ms of cooling

5.1.3 Electron beam diagnostics

The control and measurements of the main cooler parameters, like the electron-beam current intensity I_b and the different voltage measurements, did not present major difficulties.

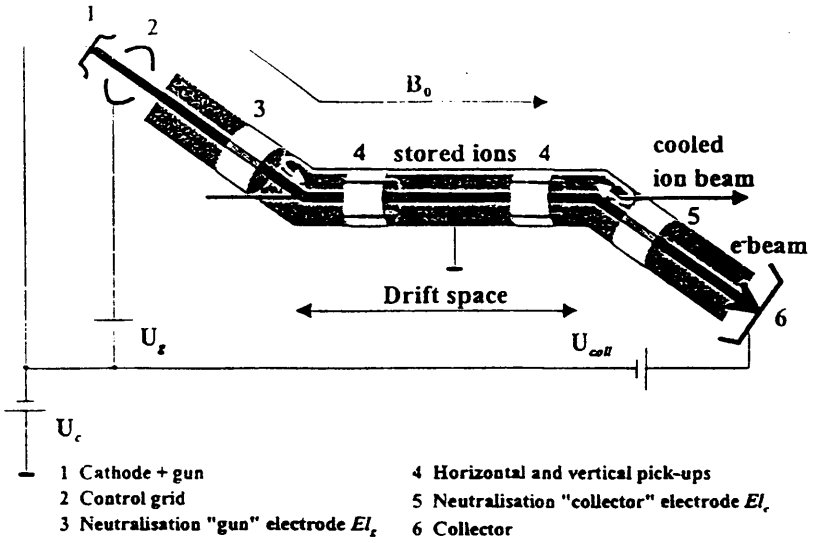

Fig. 4

For $I_b \geq 0.1$ A attention must be paid to the electron-beam stability. The stability is observed through the time of flight measurement [8] which was always in use during the experiments. It consists in measuring the phase difference between an excitation signal, applied on the neutralisation electrode, (i.e. an electrode structure that can be polarized to trap ions from the residual gas in the electron beam) on the gun side, and the signal observed on the neutralisation electrode on the collector side (Fig. 4). Stable electron velocities show up by a constant phase difference. Instabilities are due to an abrupt change of the neutralization of the electron beam. They are avoided by a beam "shaker" [9] for intensities $I_b \leq 0.5$ A. The "shaker" applies a transverse excitation signal (with a frequency in the range of 100-500 kHz) to one pair of the "pick-up electrodes" ("4" in Fig. 4) which are used as kicker for this purpose.

For intensities larger than 0.5 A there are additional difficulties [9,10] due to the build-up, in few seconds, of stored secondary electrons at the level of the grid of the electron gun. This electron cloud will reduce the nominal electron intensity controlled by the grid voltage. A way to circumvent this limitation consists in the use of a "blower" which switches off the grid potential U_g during a short time, such that the electron cloud will disappear and the nominal intensity retrieved. This technique, when used without special care, can lead to a variation in time of the electron current and, therefore, corrupt the lifetime measurement.

The accelerating voltage U_e must also be kept very stable. Indeed any voltage change introduces a shift in the ion revolution frequency which can result in errors on the lifetime estimates when the Schottky band moves out of the resolution bandwidth of the analyzer.

6. LIFETIME MEASUREMENTS

In Table 3 the main parameters of LEAR and its cooler are recalled for convenience.

Table 3 - Parameters of the experiment

Ion energy	E	[MeV/u]	4.2
Velocity factor (of ions and electrons) $\beta = v/c$			0.094
Storage ring circumference	$2\pi R$	[m]	78.54
Cooling length/circumference	η		0.02
Electron beam radius	b	[cm]	2.5
Typical electron current	I	[A]	0 - 0.2 (0.4)
e-density in cooling section	$n_e = I/e\pi b^2\beta c$	[cm^{-3}]	$1.1 \times 10^8 I$
Effective e-density per turn	$n_{eff} = \eta n_e$	[cm^{-3}]	$2.2 \times 10^6 I$
Typical longit. B-field in cooler	B	[T]	0.06

The results of our measurements are shown in Fig. 5 where lifetime of ion beams with the three charge states is plotted against the intensity of the electron cooling beam. Most of the measurements were made with the shaker on. We did not observe a strong influence of the shaker on the beam lifetime but this point was not systematically investigated. The pulser was not used, except for the following 7 points:

- 2 points at 20 mA with Pb^{53+} (squares) where the shaker was not used,
- 1 point at 420 mA with Pb^{52+} (diamonds) where the "pulser" was used with a repetition rate of 2 Hz, and
- 4 points at 440 mA and 470 mA with Pb^{54+} (triangles) where the pulser was used with a repetition rate of 0.5 Hz and 1 Hz.

These points were not taken into account when plotting the inverse of the lifetime in Fig. 6. We also do not include in the plot any points with different solenoid field settings. They do not show any significant difference to the measurements made with the "standard" electron cooling settings (B = 628 gauss). Possible "second-order" effects on this dependence need further experimental and theoretical studies.

The lifetime is influenced by the vacuum conditions in addition to the phenomena linked to electron cooling such as recombination. The corresponding decay rates ($1/\tau$) add up so that:

$$\frac{1}{\tau} = \frac{1}{\tau_{vacuum}} + \frac{1}{\tau_{recombination}}$$

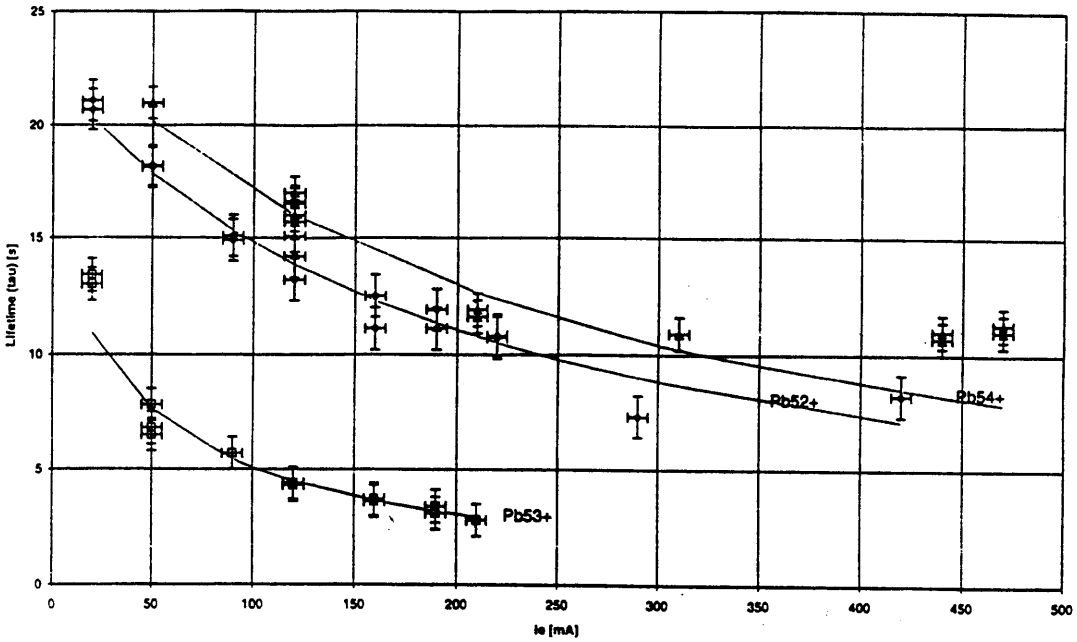

Fig. 5 - Dependence of the ion beam lifetime as a function of the electron beam current

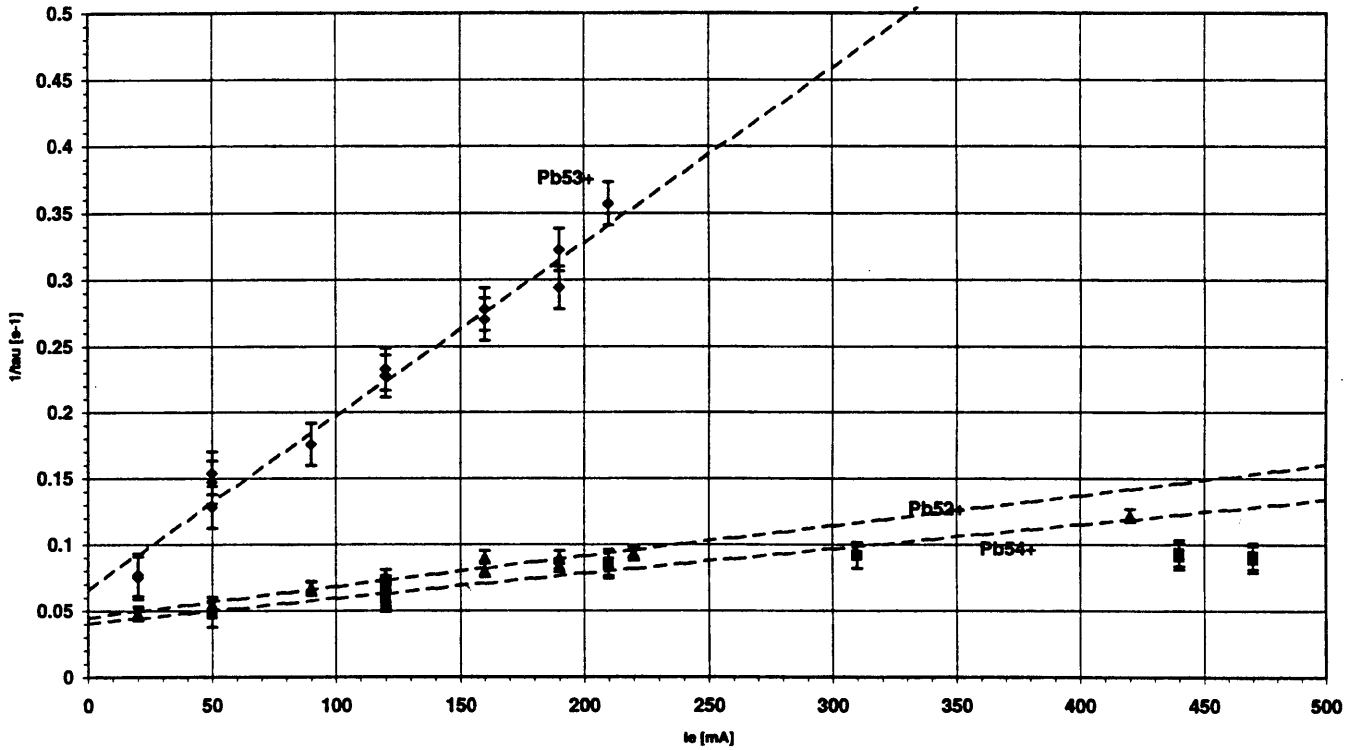

Fig. 6 - Dependence of the inverse of the lifetime as a function of the electron beam current

Therefore, from Fig. 6 we can deduce the vacuum lifetime (the zero crossing) and the lifetime due to recombination phenomena (the slope of the curves). During the experiment the LEAR vacuum conditions changed. It is for this reason that the curve for Pb^{53+} (which was measured at the beginning of the experiment) has a different zero crossing than the ones for

Pb^{54+} and Pb^{52+} (which were measured on subsequent days.) In fact, a test performed at the end of the MD gave (within the accuracy of the measurement) the same vacuum lifetime ($\tau \approx 17$ s) for all three charge states.

Subtracting the decay $1/\tau_{vac}$ due to the residual gas the three curves all cross the origin (Fig. 7). From the slope of the curves, rate coefficients $\langle \sigma v_{rel} \rangle = \alpha = (1/\tau)/n_{eff}$ can be deduced.They give the decay rate due to the presence of the electron beam normalised by the effective electron density. The effective density here is the electron density $n_e = I/e\pi b^2 \beta c$ of the cooling beam multiplied by the circumference factor η = cooler length/LEAR circumference. The normalized rates found are listed in Table 4 together with the values of "anomalously" strong recombination coefficients that were recently measured at GSI-Darmstadt.

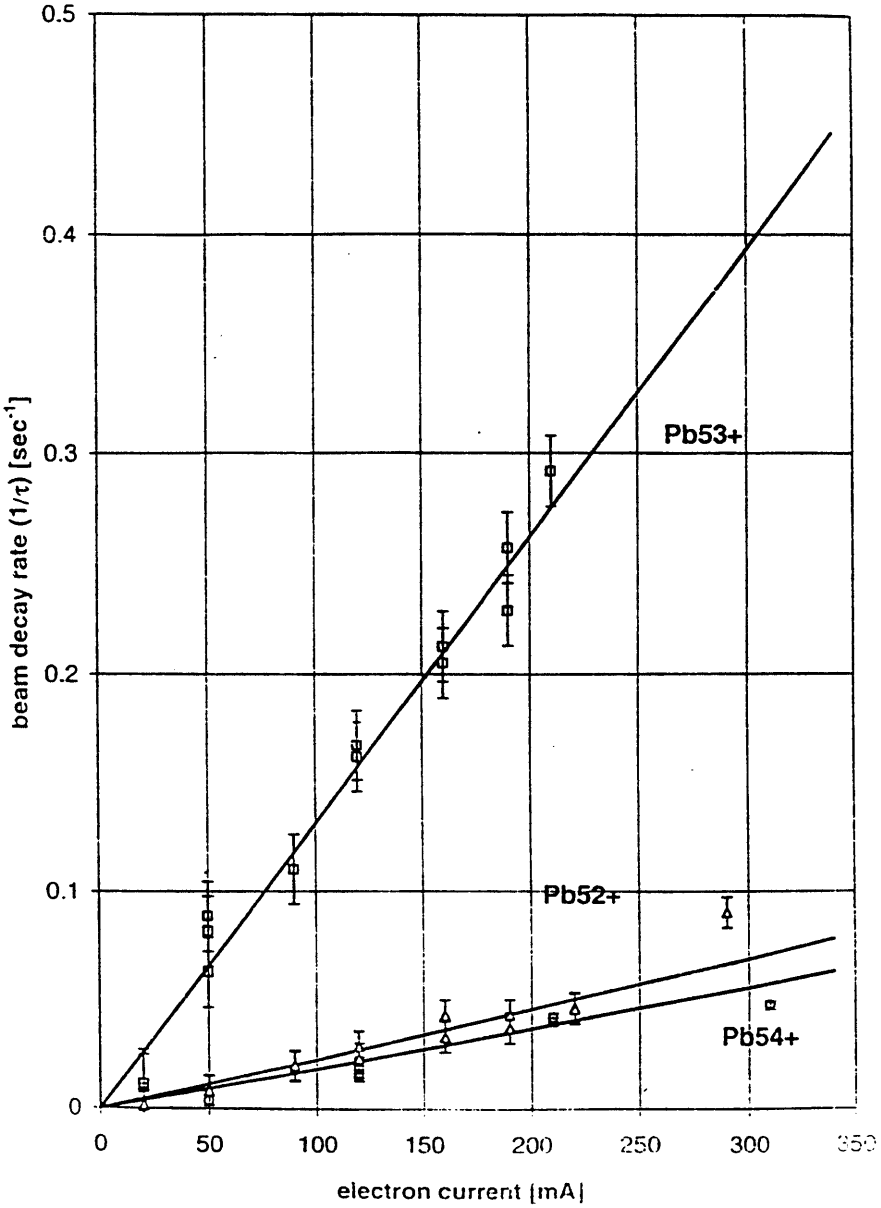

Fig. 7 - Beam decay rate (inverse of lifetime) as a function of the electron current. Compare to Fig. 6 the constant decay rate ($1/\tau \sim 1/17$ s^{-1}) due to charge exchange with the residual gas has been subtracted from the data to emphasize the decay due to recombination

Table 4 - Rate coefficients. Present results and values reported in the literature for some partially stripped ions. Included for comparison are the rates calculated for radiative capture from Bell's formula [11] taking $T_{e\perp} = 0.2$ eV and an effective ion charge $Q_{eff} = (Q+Z)/2$ [12].

Ion	Measured rate coefficient α [10^{-8} cm^3s^{-1}]	Reference	Calculated coefficient for radiative capture α [10^{-8} cm^3s^{-1}]
Pb^{52+}	11	present results (June 95)	2.25
Pb^{53+}	60	"	2.29
Pb^{54+}	9	"	2.32
U^{28+}	10	[12 - 14]	1.8
Au^{25+}	10	[13]	1.3

6.1 Comments on the results

Several observations can be made from Table 4 :

- All rates are faster than expected for radiative capture (Appendix 1).
- The rate for Pb^{53+} is 5-6 times faster than for neighbouring states Pb^{52+} and Pb^{54+}. The difference between Pb^{52+} and Pb^{54+} is not very significant.
- The rate coefficients of Pb^{52+} and Pb^{54+} resemble those of U^{28+} and Au^{25+} measured at GSI [12-14] whereas the rate of Pb^{53} is exceptionally high.

Attempts reported in the literature to explain the "anomalous" recombination by dielectronic capture [4, 12-14] are so far only partially successful. Thus after a careful examination of the possible resonances Ref. [14] concludes that the "... recombination rate of U^{28+} ions... still remains a mystery."

Our experiment is apparently the first one that explores the recombination of neighbouring charge states of the same element with electron cooling showing a marked difference in the capture cross section.

We have no explanation to offer for the higher recombination rate of Pb^{53+} except the observation that Pb^{54+} and Pb^{52+} have the possibility to arrange their remaining 28 or 30 electrons in closed shells (K, L, M for 54+; K. L, M plus the N,s sub-shell for 52+) whereas Pb^{53+} has only one out of the two electron places of the N,s sub-shell occupied. (Appendix 2).

The coefficients quoted have been derived from the decay rates for electron currents $I_b \leq$ 300 mA where one observes a good linearity of $1/\tau$ versus I_b. For larger currents the curves have a tendency to "level off" (Fig. 6). Several things can be of importance here, e.g. the space-charge potential of the electron beam, the use of the blower, and other phenomena which upset the linear relationship between electron current and density. A similar "leveling off" of the

cooling rate with electron current seems also to be present. This has to be investigated in future runs.

For all measurement points, care was taken to have good cooling in all three planes. To this end the "equilibrium" beam size and $\Delta p/p$ after about 1 s, obtained from the BIPM's and the width of the Schottky bands, was observed and optimised by fine adjustment of the cooler settings. In this way the curve for Pb^{53+} measured in December 94 could be reproduced and the "anomalous" points measured then can now be attributed to bad transverse cooling.

Finally it should be mentioned that the lifetime measurements, even after substraction of the constant decay rate due to the residual gas, yield the total rate linked to the electron cooling. We have, at present, no means to distinguish between (radiative, dielectronic, ...) recombination and other charge changing mechanisms occurring in the cooling section. We plan to install (in January/February 1996) a detector near the cooling section to observe x rays concurrent with recombination and a detector in the bending magnet downstream of the electron cooling to observe the lower charge state ions emerging from the cooler.

7. COOLING TIMES

Since there were no direct means to check the ion and electron beam alignment, the measurements given in this chapter are rough.

The longitudinal cooling time was measured with the help of the longitudinal Schottky pick-up by observing the width of the band at a given harmonic (again $h = 100$ was chosen) of the revolution frequency. The relative momentum deviation $\Delta p/p$ was reduced from 10^{-3} to 10^{-4} in less than 100 ms for an electron beam intensity $I_b \cong 120$ mA.

The transverse cooling time is estimated from the beam rms with σ_h and σ_v obtained from the BIPM's. Figure 8 gives the evolution of σ_h [mm] and σ_v [mm] versus time [ms]. In both cases $I_b = 120$ mA and the charge state in the example displayed in Fig. 8 is 54+.

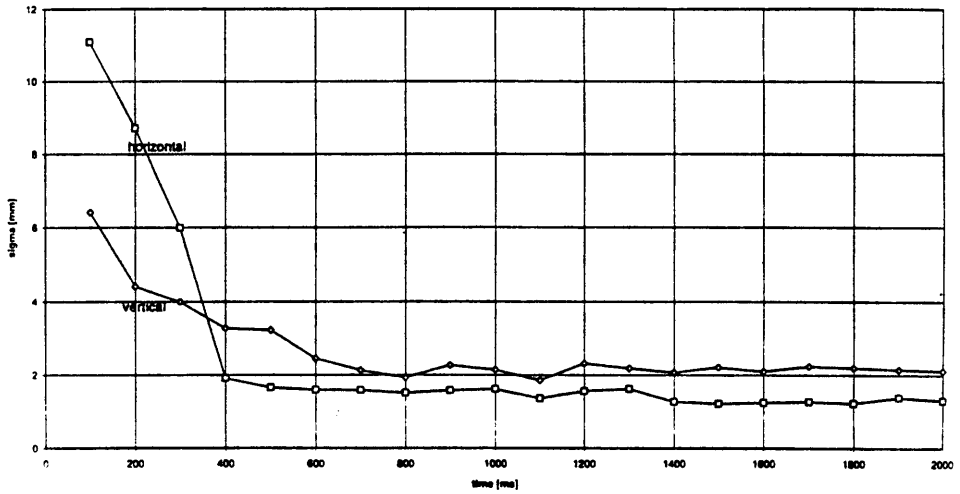

Fig. 8 - Evolution of σ_H (mm) and σ_V (mm) versus time (ms)

7.1 Comments on the Transverse Cooling Time

Initially the ion beam occupies the entire LEAR acceptance as shown previously in Fig. 3 (top figure at t = 100 ms) Therefore, the transverse shape changes drastically during cooling such that it is difficult to interpret the computed values of the rms width in terms of emittance cooling.

However, it can be seen that the beam width is reduced from 8 to 2 mm in about 400 ms, i.e. the time needed for the emittance to be reduced by a factor 16 is about 400 ms.

We had the impression that the ions injected at large radius are not captured by the cooling process and are therefore lost. In the future, the BIPM's sum signals have to be carefully checked since these losses will have to be taken into account to evaluate the stacking performance.

8. REQUESTS FOR FUTURE RUNS

- Linac and Injection line:

  More SEM-grids with slow electronics are needed. A current transformer would be very helpful. Measurements with Pb ions in the E0 line should be scheduled for Aug.-Oct. 1995. Pb^{55+} ions for further studies of the recombination for the run in December 1995 could be interesting.

- LEAR:

  Check the accuracy of the BIPM's (sum signals, rms computation...),
  Residual gas analysis, also in SS4,
  Detector of the lost ions in the bending magnet, BHN3 (to be installed in the January 1996 shut down),
  x-ray detector at the level of the cooler or at the location of HØ beam.
  Improvement of the vacuum for future runs (average pressure and/or gas composition improvement by a factor 2-3. This would permit some simple stacking with the present repetition rate of the linac).

9. CONCLUSION

The experiment clearly indicates that Pb^{52+} and Pb^{54+} are less liable to loss in connection with electron cooling than Pb^{53+} ions. With good vacuum conditions the $1/e$ lifetime at 400 mA electron current is at least 10 s compared to 2 s for Pb^{53+}. This will permit us to cool and store Pb^{54+} (or Pb^{52+}) during 2-4 s, as proposed in Ref. [1], with acceptable losses. The linac can deliver all three charge states with practically equal intensities. It is therefore proposed to base the project [1] on the storage of Pb^{54+} which is more easily transferred through the bends of the E0 line than Pb^{52+}. The future tests of cooling and accumulation will concentrate on this charge state. Investigation of the transfer line, the injection into LEAR and the influence of the LEAR

optics on cooling will have high priority for the tests scheduled for December 1995 and for next year.

The difference between the neighbouring charge states is interesting for recombination theories. Our measurement yields the total rate coefficient linked to the electron cooling beam. We plan to install a monitor to detect x rays characteristic for the recombination. In addition "beam loss monitors" to observe the lower charge ions emerging from the cooling section are under study.

The difference in rate coefficients applies to co-moving electrons (zero c.m. energy). The charge exchange with the residual gas was -within the ±15% accuracy of the experiment- the same for all three charge states.

REFERENCES

[1] P. Lefèvre and D. Möhl, *A low energy accumulation ring of ions for LHC feasibility study*, CERN-PS 93-62/LHC Note 259 (1993) and, *Lead ion accumulation scheme for LHC*, in: Proc. Workshop on Beam Cooling and Related Topics (Montreux, 1993), ed. J. Bosser (CERN 94-03, 1994) p. 411.

[2] J. Bosser, G. Tranquille, I. Meshkov, *Magnetized electron cooling time for heavy ions*, PS AR/Note 94-11.

[3] S. Baird, J. Bosser, M. Chanel, J. Duran, R. Giannini, P. Lefèvre, R. Ley, R. Maccaferri, S. Maury, I. Meshkov, D. Möhl, G. Molinari, F. Motsch, H. Mulder, U. Oeftiger, J.C. Perrier, E. Roux, G. Tranquille, F. Varenne, *First electron cooling tests with Pb^{53+} Ions* (Performed in December 1994), PS/AR/Note 95-06 (MD) (1995).

[4] H. Beyer, D. Liesen and O. Guzman, *On the total recombination between cooling electrons and heavy ion*, Part. Acc. 24 (1989), p. 163,
A. Müller, *Electron-ion recombination phenomena*, in: Proc. Workshop on Recombination of Atomic Ions (Newcastle, 1991), eds. W. Graham et al. (Plenum Press, New York, 1992) p. 155.

[5] D.J. Warner, *Heavy Ion Linac for the CERN lead ion facility*, in: Proc. 1994 Linac Conf. (Tsukuba), Vol. 2, eds. T. Takata, W. Yamazaki and K. Nakahara, p. 654.
H. Haseroth, The CERN heavy ion accelerating facility, in: Proc. 1995 Part. Acc. Conf. (Dallas), to be published.

[6] E. Baron, M. Bajard and C. Ricaud, *Charge exchange of very heavy ions in carbon foils*, Nucl. Instr. Methods A238 (1993), p. 117.

[7] B. Franzke, *Vacuum requirements for heavy ion synchrotrons*, Procs. of the 1981 Part. Acc. Conf. IEEE Trans. Nucl. Sci., Vol. NS-28, No.3, June 1981, p. 2116.

[8] J. Bosser, I. Meshkov, D. Möhl, V. Parkhomchuk, E. Syresin, G. Tranquille, *Neutralization of the LEAR-ECOOL electron-beam space charge*, PS/AR/Note 93-08 (1993).

[9] J. Bosser, F. Caspers, M. Chanel, R. Ley, R. Maccaferri, S. Maury, I. Meshkov, G. Molinari, V. Polyakov, A. Smirnov, O. Stepashkin, E. Syresin, G. Tranquille, F. Varenne, *Neutralisation of the LEAR electron cooling beam: Experimental results*,

CERN/PS 95-17 (AR) (1995). To be published in: Proc. of the 1995 Part. Acc. Conf. (Dallas).

[10] I.N. Meshkov, V. Poliakov, A. Smirnov, E. Seyreysin, R. Lapik, I.A. Seleznev, A. Zapunjako, M. Zavaraznov, J. Bosser, R. Ley, G. Tranquille, *The variable current gun: The parameter tests and the first electron cooling experiments at LEAR*, NIM A-355 (1995) p. 208.

[11] K. Kilian and D. Möhl, *Phase-space cooling of ion beams*, Lecture Notes in Phys. 178 (1983), p. 163. (Preprint CERN-EP 82-214).

[12] A. Müller, S. Schennach, M. Wagner, J. Haselbauer, O. Uwira and W. Spies, *Recombination of free electrons with ions*, Physica Scripta T37 (1991), p. 62.

[13] A. Müller et al., *Radiative and dielectronic recombination*, in: Proc. Symposium on Cooler Rings (Tokyo, 1990), eds. T. Katayama and A. Noda (World Scientific, London, 1991) p. 248.

[14] O. Uwira, A. Müller, W. Spies, A. Frank, J. Linkemann, L. Empacher, P.H. Mokler, R. Becker, M. Kleinod, *Recombination of electrons with U^{28+} ions in a dense, cold electron target*, in: GSI Scientific Report 1994, GSI 94-1 (March 1995), ed. U. Grundiger, p. 137.

[15] The LHC Study Group, eds. Y. Baconnier, G. Brianti, Ph. Lebrun, A. Mathewson, LHC, *The Large Hadron Collider accelerator project*, Report CERN/AC/93-03 (LHC) (1993).

[16] M. Bell, J.S. Bell, *Capture of cooling electrons by cool protons*, Part. Acc. 12 (1981), , p.49 (Preprint CERN TH-3034 1981).

APPENDIX 1

Radiative Recombination

Bell's formula [16] generalised for fully stripped heavy ions [11] can be written in the following form :

$$\alpha = \frac{3.02\ Z^2}{\sqrt{kT_\perp}}\left[\ell n\left(\frac{11.3\ Z}{\sqrt{kT_\perp}} + 0.14\left(\frac{kT_\perp}{Z^2}\right)^{1/3}\right)\right] \times 10^{-13}\ cm^3\ s^{-1}$$

Here $kT_\perp$ is the transverse temperature [in eV], given by the electron temperature once the ion beam is cooled. A flattened distribution ($T_\perp >> T_{||}$) has been assumed. A rough approximation for partially stripped ions is to insert the charge state Q of the ion in the place of Z. As on improved approximation, ref. [12] suggests to use the "effective charge"

$$Q_{eff} = \frac{Q+Z}{2}$$

This prescription has been used, to calculate the rates for radiative capture given in Table 4.

APPENDIX 2

The atomic structures of a Pb atom are shown in Table A.1.

Table A.1 - Pb atomic structures

Shell	Subshell	No. of e^- in subshell	Total member of e^-
K ($n = 1$)	s	2	2 (He)
L ($n = 2$)	s	2	
	p	6	10 (Ne)
M ($n = 3$)	s	2	
	p	6	18 (Ar)
	d	10	28
N ($n = 4$)	s	2	30
	p	6	36 (Kr)
	d	10	46
	f	14	
0 ($n = 5$)	s	2	
	p	6	68
	d	10	78
P ($n = 6$)	s	2	
	p	2	82

Table A.2 shows the cumulative ionization energy together with the shell and subshell configuration.

In a Pb^{52+} ion 30 electrons remain bound to the nucleus. We deduce from Table A.1 that the two lowest energy electrons belong to the N ($n = 4$), s state. This subshell is fully occupied with 2 electrons. For Pb^{53+} only one electron place in this sub-shell is occupied which may give rise to a stronger capture cross-section.

Considering Pb^{54+}, we see that it can arrange its 28 electrons in the shells: K,L,M which are then completed. This again may lead to more stable ion, less sensitive to recombination. Also from Table A.2 the difference in ionization energy between Pb^{53+} and Pb^{54+}, is relatively large, whereas the difference between Pb^{52+} and Pb^{53+} is relatively small.

Table A-2. Ionization potentials of Pb atom

Atomic Data Vol. 2 (p. 63-99) 1970 Carlson et al

PB Z = 82.

ION	CONFIG	IP, EV
NEUTRAL	(6P-)2	6.906E 00
1+	(6P-)1	1.559E 01
2+	(6S+)2	3.227E 01
3+	(6S+)1	4.359E 01
4+	(5D+)6	6.721E 01
5+	(5D+)5	8.799E 01
6+	(5D+)4	1.087E 02
7+	(5D+)3	1.295E 02
8+	(5D+)2	1.503E 02
9+	(5D+)1	1.710E 02
10+	(5D-)4	1.947E 02
11+	(5D-)3	2.161E 02
12+	(5D-)2	2.375E 02
13+	(5D-)1	2.588E 02
14+	(5P+)4	3.468E 02
15+	(5P+)3	3.737E 02
16+	(5P+)2	4.006E 02
17+	(5P+)1	4.275E 02
18+	(5P-)2	4.776E 02
19+	(5P-)1	5.071E 02
20+	(4F+)8	5.718E 02
21+	(5S+)2	6.143E 02
22+	(5S+)1	6.458E 02
23+	(4F+)7	6.946E 02
24+	(4F+)6	7.544E 02
25+	(4F+)5	8.142E 02
26+	(4F+)4	8.740E 02
27+	(4F+)3	9.338E 02
28+	(4F+)2	9.936E 02
29+	(4F+)1	1.053E 03
30+	(4F-)6	1.113E 03
31+	(4F-)5	1.179E 03
32+	(4F-)4	1.240E 03
33+	(4F-)3	1.300E 03
34+	(4F-)2	1.361E 03
35+	(4F-)1	1.421E 03
36+	(4D+)6	1.758E 03
37+	(4D+)5	1.820E 03
38+	(4D+)4	1.883E 03
39+	(4D+)3	1.946E 03
40+	(4D+)2	2.008E 03
41+	(4D+)1	2.071E 03
42+	(4D-)4	2.157E 03
43+	(4D-)3	2.221E 03
44+	(4D-)2	2.285E 03
45+	(4D-)1	2.350E 03
46+	(4P+)4	2.625E 03
47+	(4P+)3	2.690E 03
48+	(4P+)2	2.755E 03
49+	(4P+)1	2.821E 03
50+	(4P-)2	3.008E 03
51+	(4P-)1	3.079E 03
52+	(4S+)2	3.279E 03
53+	(4S+)1	3.350E 03
54+	(3D+)6	5.026E 03
55+	(3D+)5	5.194E 03
56+	(3D+)4	5.362E 03
57+	(3D+)3	5.530E 03
58+	(3D+)2	5.698E 03
59+	(3D+)1	5.866E 03
60+	(3D-)4	6.139E 03
61+	(3D-)3	6.312E 03
62+	(3D-)2	6.485E 03
63+	(3D-)1	6.658E 03
64+	(3P+)4	7.122E 03
65+	(3P+)3	7.273E 03
66+	(3P+)2	7.423E 03
67+	(3P+)1	7.574E 03
68+	(3P-)2	8.368E 03
69+	(3P-)1	8.534E 03
70+	(3S+)2	8.891E 03
71+	(3S+)1	9.048E 03
72+	(2P+)4	1.858E 04
73+	(2P+)3	1.901E 04
74+	(2P+)2	1.944E 04
75+	(2P+)1	1.986E 04
76+	(2P-)2	2.248E 04
77+	(2P-)1	2.298E 04
78+	(2S+)2	2.385E 04
79+	(2S+)1	2.429E 04
80+	(1S+)2	9.755E 04
81+	(1S+)1	9.925E 04